GS-12-004

Fifth International Symposium on Cavitation (CAV2003)
Osaka, Japan, November 1-4, 2003

SIMULATION OF STEADY AND UNSTEADY CAVITATION ON A MARINE PROPELLER USING A RANS CFD CODE

Takayuki WATANABE
The University of Tokyo, Tokyo, Japan
takayuki@fluidlab.naoe.t.u-tokyo.ac.jp

Takafumi KAWAMURA
The University of Tokyo, Tokyo, Japan
kawamura@fluidlab.naoe.t.u-tokyo.ac.jp

Yoshihisa TAKEKOSHI
The University of Tokyo, Tokyo, Japan
takekosi@fluidlab.naoe.t.u-tokyo.ac.jp

Masatsugu MAEDA
The University of Tokyo, Tokyo, Japan
maeda@fluidlab.naoe.t.u-tokyo.ac.jp

Shin Hyung RHEE
Fluent Inc., Lebanon, NH, USA
shr@fluent.com

ABSTRACT

RANS simulations of flow around two different conventional propellers were carried out at non-cavitating and cavitating operating conditions using the multiphase flow model based on the "full cavitation model" proposed by Singhal et al. [1]. The predicted values of the thrust and torque coefficients in uniform flow were in a good agreement with the measurements in cavitating and non-cavitating conditions.

Unsteady flow around Seiun-maru conventional propeller in a non-uniform ship wake was also computed. The fluctuation of the blade surface pressure was compared with the measurement, and the agreement was qualitatively good.

The overall results suggest that the present approach can complement the model experiments for actual cavitating propeller design procedures.

INTRODUCTION

Reynolds Averaged Navier-Stokes (RANS) methods have attracted attention as a practical tool in place of conventional methods based on the potential theory. RANS methods have been successfully applied not only to viscous flow around ship hulls but also to marine propellers [2-3]. However, since structure grids were used in most cases, computational results are limited for steady flow in open water conditions. For future extension to coupled simulation with a ship hull and a rudder, the use of structured grids can be a substantial barrier. Also, due to the complexity of propeller geometry, it is not easy to generate sufficiently fine grid to resolve the tip vortex [2]. Therefore, we think that the use of unstructured mesh is necessary for future extension to hull-propeller interaction and improvement of accuracy.

Funeno [3-6] has applied unstructured grid technique to the flow around the Seiun-maru highly-skewed propeller. The agreement with experiment was good both for steady and unsteady conditions, but the scheme for the grid generation was very complicated. In that work, the computational domain was decomposed into 46 pieces, and block-structured grid was generated for each sub-domain.

In this paper, we investigate the use of simpler grid system which mainly consists of tetrahedral cells except for the region near the body surface, for which prismatic cells are used for resolving the boundary layer. Using this hybrid mesh, viscous flows around two different marine propellers are simulated for uniform and non-uniform inflow conditions, and the accuracy is discussed.

For RANS methods to replace or complement model experiments of marine propellers, consideration of cavitation is necessary, since it is as important as the efficiency in propeller design. Although numerical simulation methods of cavitation have been developed in the last decade [7], they have not been applied propeller flow. Thus the second objective of this study is to investigate the application of cavitation models to steady and unsteady flow around a marine propeller. As the cavitation model, the "full cavitation model" developed by Singhal et al [1] was used in this study.

NOMENCLATURE

C_{pn}: Propeller pressure coefficient $C_{pn} = \dfrac{p - p_\infty}{\frac{1}{2}\rho(nD)^2}$

D : Propeller diameter in [m]

J : Propeller advance coefficient $J = \dfrac{V_a}{nD}$

K_T : Propeller thrust coefficient $K_T = \dfrac{Thrust}{\rho n^2 D^4}$

K_Q : Propeller torque coefficient $K_Q = \dfrac{Torque}{\rho n^2 D^5}$

n : Propeller revolution in [1/s]
p : Static pressure
p_v : Vapor pressure
p_∞ : Static pressure at far field

R_n : Reynolds number $R_n = \dfrac{nD^2}{\nu}$
V_a : Propeller advance velocity in [m/s]
ρ : Density of water

σ : Cavitation number $\sigma = \dfrac{p_\infty - p_v}{\frac{1}{2}\rho(nD)^2}$

NUMERICAL METHOD

As the RANS solver, we used a commercial CFD code Fluent version 6.1. Fluent is an unstructured mesh based finite volume code, and detailed descriptions of the numerical method are found in the Fluent 6.1 Users Guide [8] or in publications such as Kim [9-10]. The k-ω turbulence model [11] was chosen as the turbulence model. A segregated solver with SIMPLE as the velocity-pressure coupling algorithm was selected, and QUICK scheme was used for the discretization of the momentum equation in this study. The discretized equations are solved using pointwise Gauss-Seidel iterations, and algebraic multi-grid method accelerates the solution convergence.

In Fluent version 6.1 the full cavitation model developed by Singhal et al. [1] is implemented with an extension to include the influence of slip velocity between the liquid and gas phases. However, since the slip velocity model was switched off in this study, the cavitation model is essentially identical to the original full cavitation model by Singhal et al.

The non-uniform inflow condition was implemented through the "user defined function (UDF)" feature of Fluent. The measured wake distribution at irregular points is interpolated to arbitrary mesh positions.

PROPELLER MODELS

In this paper, two conventional type propeller models were used for investigations. One is the MP017 propeller designed at the University of Tokyo and detailed measurements are reported in Yamaguchi et al. [12]. The propeller can be characterized by the flat pressure distribution on the backside and better cavitation characteristics than the conventional MAU type propeller on which it is based. The other one is Seiun-maru propeller, which is known for abundant experimental data, and often used as a bench mark of propeller flow simulations [6]. The geometries and the principal particulars of the two propeller models are shown in Figure 1 and Table 1, respectively.

Preliminary computations for MP017 showed that the accuracy in the performance prediction was improved only by 0.3% by the accurate modeling of the boss and shaft. Hence the boss and shaft geometries were simplified for the Seiun-maru propeller.

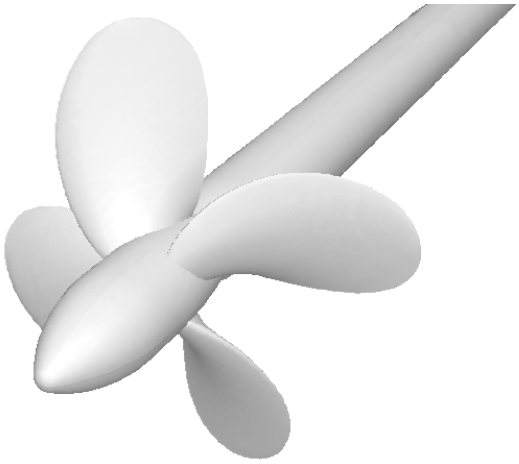

(a) MP017

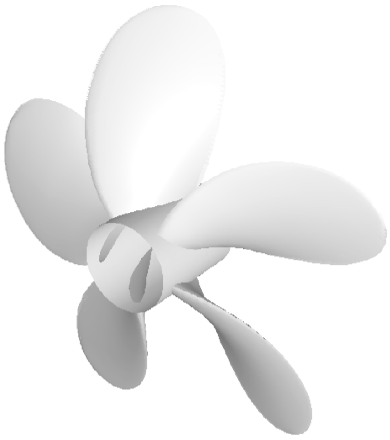

(b) Seiun-maru

Figure 1 Geometries of MP017 and Seiun-maru conventional propeller

Table 1 Principal particulars of MP017 and Seiun-maru conventional propeller

Model name	MP017	Seiun-maru
Number of blades	4	5
Diameter [m]	0.2143	0.4000
Boss ratio	0.1800	0.1972
Pitch ratio at 0.7R	0.8493	0.950
Expanded area ratio	0.6000	0.650
Skew [m]	0.01257	0.183
Rake [deg.]	10.00	6.0

GRID GENERATION

A hybrid mesh was generated using Fluent preprocessors GAMBIT and TGrid. First, the blade surface was meshed with triangles. The region around the root, tip, and blade edges was meshed with smaller triangles, i.e., with sides of approximately 0.001*D*, while the inner region was filled with appropriately growing triangles. Once the blade surface was meshed, the other surfaces were meshed with larger triangles, i.e., with sides of up to 0.1*D*. In order to resolve the turbulent boundary layer on the solid surfaces, it is best to have growing prismatic cells from the blade and hub surface. This was done using TGrid, which is more specialized in hybrid mesh generation than GAMBIT. The surface mesh generated in GAMBIT was imported into TGrid. Then four layers of prismatic cells were attached to the blade and hub surface. The first cell height off the solid surface was approximately 0.00001*D*, which is 3 to 50 in terms of y^+, and the stretching ratio of the layers was 1.1. Finally the remaining region in the domain was filled with tetrahedral cells. The number of cells in this mesh was about 400,000. Figures 2-3 show the surface mesh on the blade and hub surface. Due to the aspect ratio limit with triangular faces, unstructured meshing approach generally results in a larger number of cells near the blade edges, compared to structured meshing approach. Note that this is a configuration in the cavitation tunnel, so the flow direction is from the lower-left to the upper-right corner of the Figure 2.

For steady flow simulation, the computational domain was created as one passage surrounding a blade: inlet at 1.5*D* upstream, where *D* is the propeller diameter; exit at 3.5*D* downstream; solid surfaces on the blade and hub, centered at the coordinate system origin and aligned with uniform inflow; outer boundary at 1.4*D* from the hub axis; and two rotationally periodic boundaries with 90° in between for four bladed MP017 and 72° in between for five bladed Seiun-maru propeller. Boundary conditions were set to simulate the flow around a rotating propeller in the open water: on the inlet boundary, velocity components of uniform stream with the given inflow speed were imposed; on the exit boundary, the static pressure was set to a constant value, zero in non-cavitating cases, while other variables were extrapolated; on the outer boundary, the slip boundary condition was imposed, i.e., zero normal velocity component with extrapolated tangential velocity components and static pressure; on the blade and hub surface, the no slip condition was imposed; and on the periodic boundaries, rotational periodicity was ensured. Figure 3 shows the computational domain and boundary condition used for the steady flow simulation.

Unsteady flow simulation in non-uniform ship wake was carried out for Seiun-maru propeller using the sliding mesh technique implemented in Fluent. As shown in Figure 4, the computational domain is split into global stationary part and moving part which rotates with the propeller. A simple cylindrical mesh was generated for the global stationary block. At the inlet boundary of the stationary block, the axial component of the measured nominal wake distribution shown in Figure 5 was imposed using the UDF feature of Fluent. The rotational block around the propeller was meshed in the same manner as in the steady flow case. However, since periodic boundary conditions can not be used, the full propeller geometry with five blades was meshed for the unsteady case. Figure 6 shows the surface mesh for the Seiun-maru propeller. A total of 1,579,800 cells, 1,091,100 in the rotational block and 448,700 in the stationary block were used for the simulation. In the case of the unsteady flow, the inlet, outlet and radial boundaries were located 2.0D, 5.0D and 3.0D away from the rotation axis at the blade generator line.

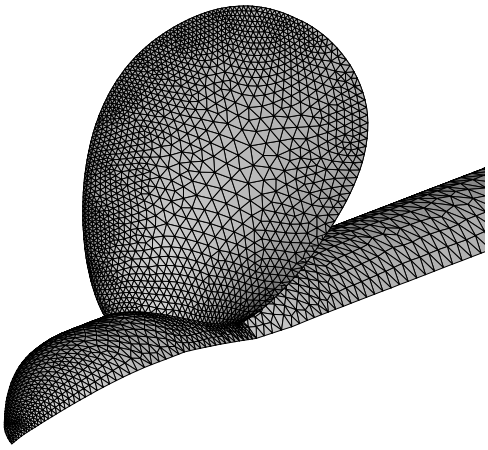

Figure 2 Surface mesh for MP017 propeller

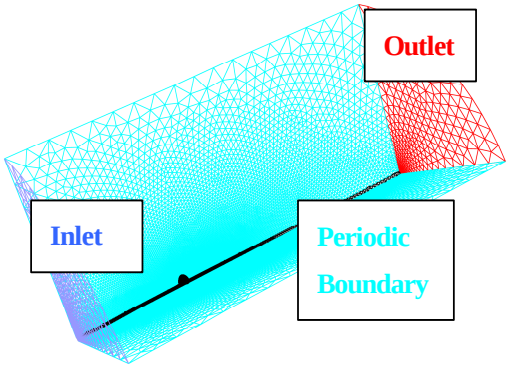

Figure 3 Arrangement of global grids around propeller for the steady flow simulation

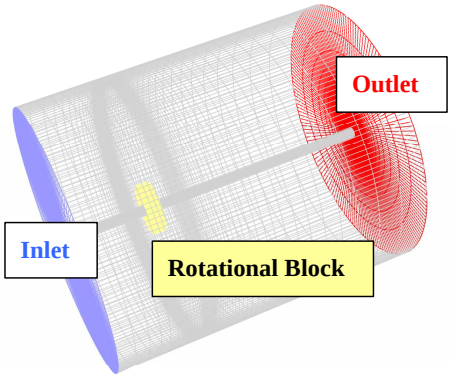

Figure 4 Arrangement of global grids around propeller for the unsteady flow simulation

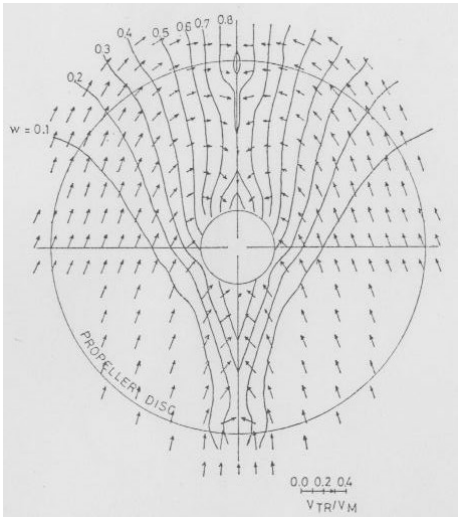

Figure 5 Measured nominal wake distribution used for unsteady simulation of Seiun-maru propeller

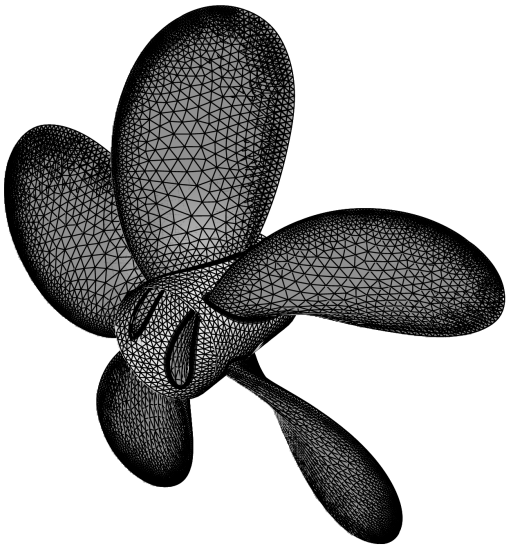

Figure 6 Surface mesh for Seiun-maru propeller

RESULTS

Simulation of propeller in uniform flow

For validation of the numerical method, computational results are compared with the experimental data. The experiment for the MP017 model was carried out at the Propeller Cavitation Tunnel of the University of Tokyo by the authors, while the experimental data for the Seiun-maru propeller was obtained by Ukon et al. [13]. The operating condition in the numerical simulation is set so as to match the condition in the experiments. For the MP017 propeller, rotation n is set to 25 rps (R_n=1.2$\times$ 10^6), and for the Seiun-maru propeller, n is set to 3.63 rps (R_n=5.8 $\times$ 10^5). A wide range of advance coefficient, $J = V_a / nD$, was considered, i.e., $0.23 \le J \le 0.90$. The value of J was varied by increasing or decreasing V_a, while n is kept constant.

Figures 7 and 8 show the curves of K_T and K_Q versus J along with the corresponding experimental values. In the figures, the red lines show present calculated data and the green dashed lines show the experimental data for comparison. For both propellers overall agreement is good, especially the error in the prediction of K_T is less than 2% over the wide range of the advance coefficient J. However, the error in K_Q is larger than in K_T. K_Q was overestimated by 7% for the MP017 propeller and 6% for the Seiun-maru propeller. This tendency that K_Q is overpredicted seems to be prevalent in most of the RANS CFD simulation for marine propellers [3, 14]. Further validation studies using reliable experimental data are recommended to clarify the reason for this discrepancy.

Fig. 9 shows chordwise distribution of the pressure coefficient on the Seiun-maru propeller at 0.7R for three different advance coefficient conditions. In the same way as for the previous figures, the red lines show present results by CFD and the green dashed lines show the experimental data, and additionally, the blue dashed lines show caculated results by Koyama's program [15] (One of the Mode Function Method programs based on the propeller lifting surface theory). Overall agreement is good, but the difference from the experimental data seems to be larger on the face side. This tendency is clearer at smaller advance coefficient as shown in Figure 9 (a) and (b).

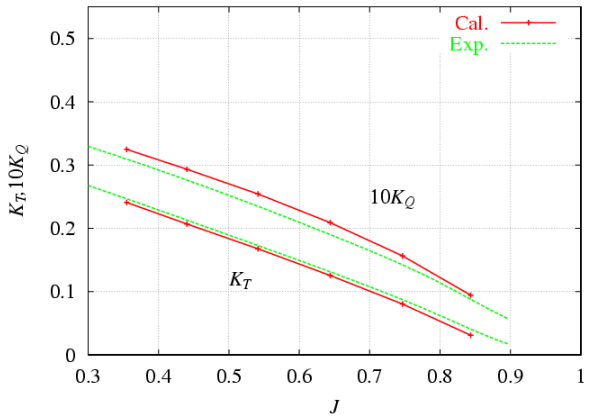

Figure 7 Computed and measured performance of MP017 propeller model in open water

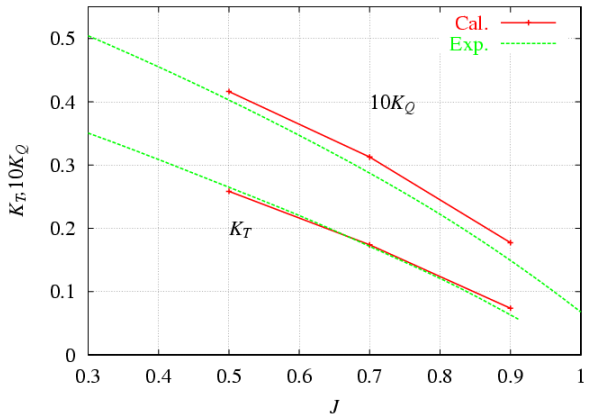

Figure 8 Computed and measured performance of Seiun-maru propeller model in open water

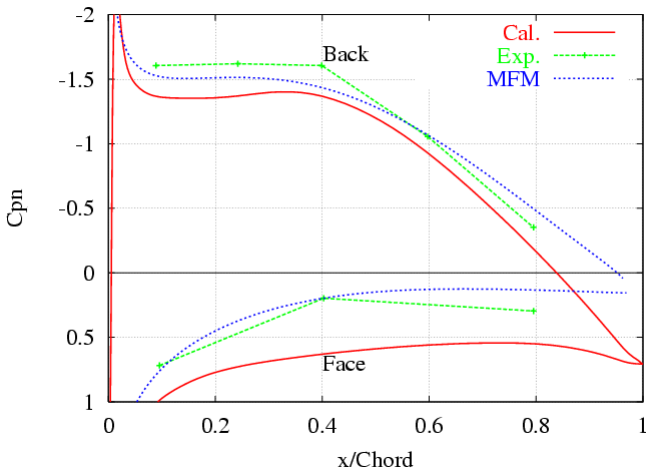

(a) *J*=0.5

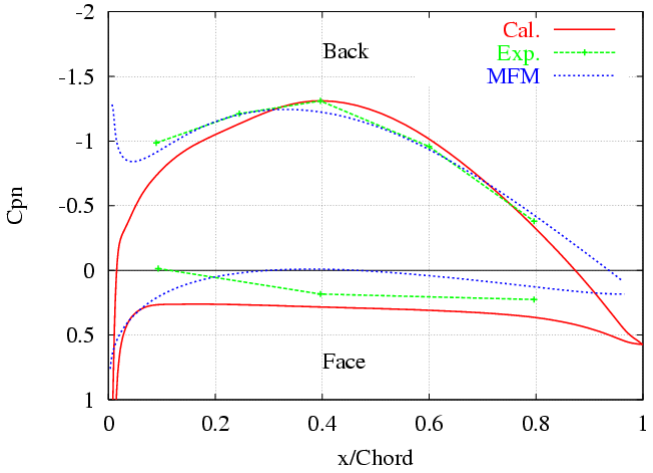

(b) *J*=0.7

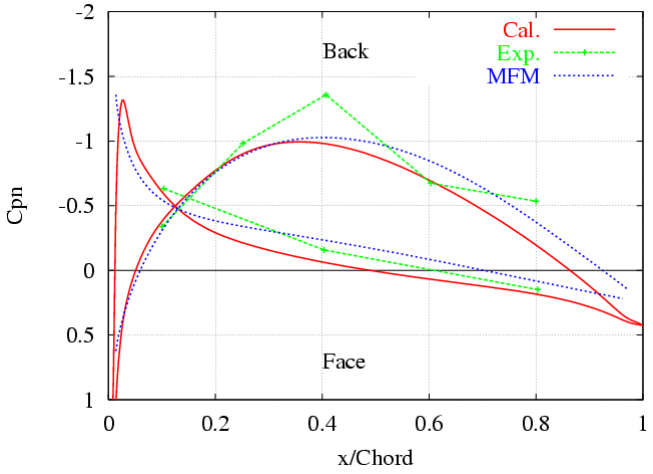

(c) *J*=0.9

Figure 9 Chordwise distribution of Cp on the Seiun-maru propeller at 0.7*R* for (a) *J*=0.5, (b) *J*=0.7, and (c) *J*=0.9

Simulation of propeller in non-uniform wake

Unsteady flow simulation in a non-uniform wake was carried out for the Seiun-maru propeller. The time step size was set to 0.000765 [sec.], which corresponds to the rotation angle of 1.0 degree. Figure 10 shows pressure coefficient contours on the back side at two different rotation angles. The pressure distribution changes depending on the blade position. The peak of the negative pressure on the back side is largest when the blade is at the top position where the axial flow velocity is the smallest. Figure 11 shows the pressure distribution on the blade surface at 0.7*R* at two different rotation angles 0 and 90 degrees. The angle of 0 degree corresponds to the top position and the angle increases in the counter-clockwise direction. It is shown that a reasonable agreement is obtained also for the unsteady case. Figure 12 shows the variation of the pressure coefficient on the blade surface during a rotation in the non-uniform flow. The variation is well predicted as a whole, but the small peak around the rotation angle θ=180 degree is not reproduced in the CFD simulation. This is probably due to the insufficient resolution in the wake, and further investigations are being carried out at present.

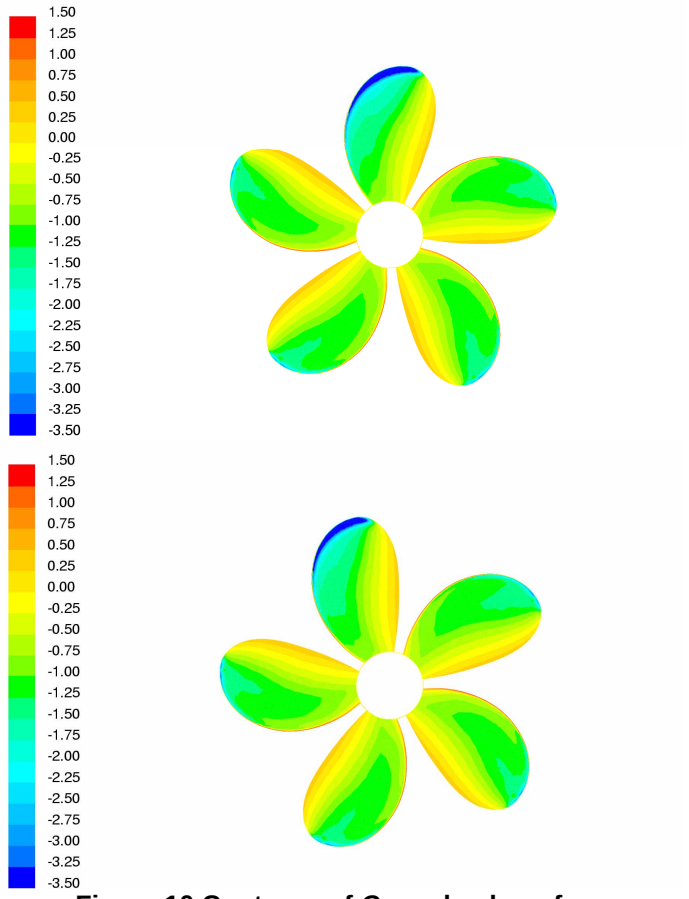

Figure 10 Contours of *Cp* on back surface of Seiun-maru propeller in non-uniform flow

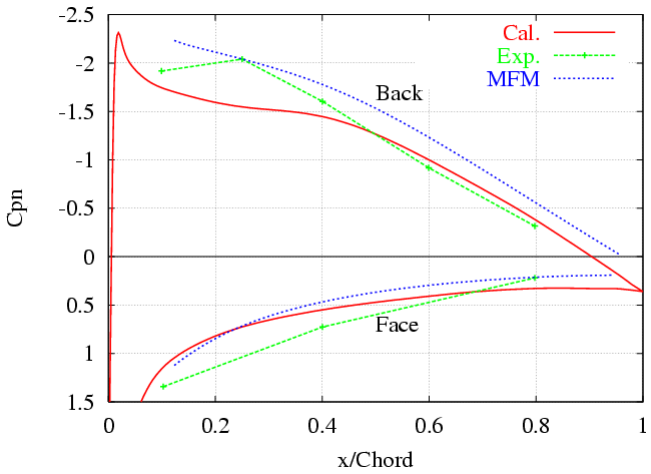

(a) 0[deg.]

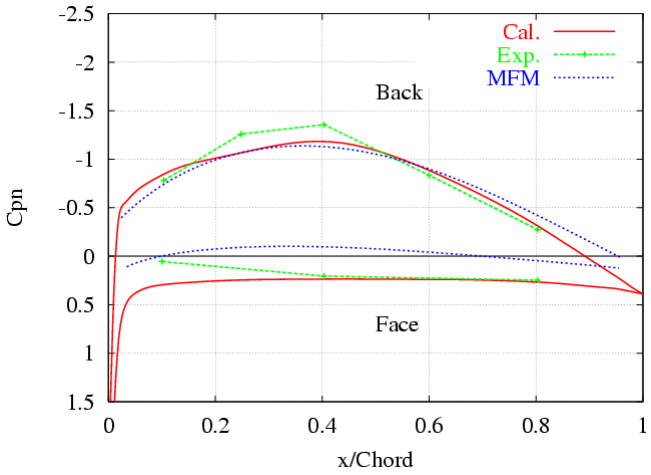

(b) 90[deg.]

Figure 11 Chordwise distribution of *Cp* on the Seiun-maru propeller in non-uniform flow at two different rotation angles (a) 0[deg.] and (b) 90[deg.]

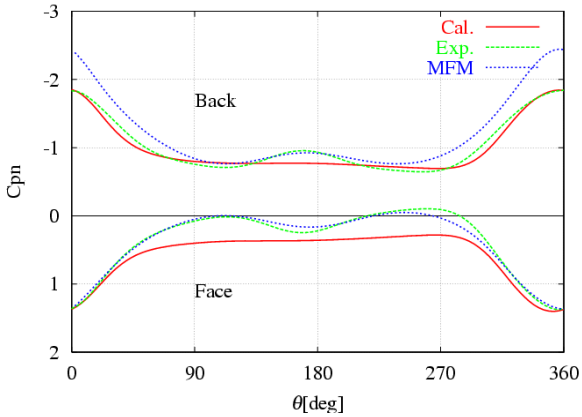

(a) *r/R*=0.7, *x/C*=0.1

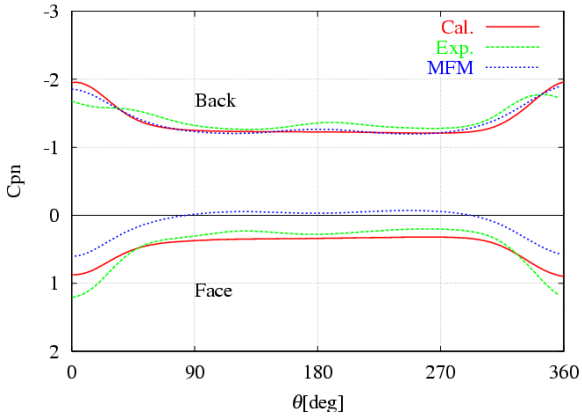

(b) *r/R*=0.9, *x/C*=0.4

Figure 12 Variation of the *Cp* on the blade surface of Seiun-maru propeller during a rotation in non-uniform flow

Simulation of cavitating marine propeller

Boundary conditions for the cavitating cases were set in the same way as for the non-cavitating cases. The only difference is on the exit boundary, where the constant exit pressure was set to match the given cavitation number σ.

Figure 13 presents the curves of K_T and K_Q vs. σ at J=0.2 and 0.55, along with corresponding measured values. The thrust breakdown is one of the major issues in cavitating propellers. At the large angle of attack, J=0.2, both K_T and K_Q start decreasing upon the onset of cavitation at σ=2.0. This behavior is quantitatively well reproduced in the present simulation. However, at the small angle of attack, J=0.55, there is discrepancy between the measured and simulated values at lower σ 's. The measured K_T and K_Q remain almost constant although the occurrence of cavitation is visually and acoustically apparent at σ below 2.0, while the simulated K_T and K_Q over-predict the decrease in this range. It was also noticed that the predicted length of the cavity is smaller than in the experiment. It is very likely that this is the reason for the discrepancy. Generally for a lifting foil at a small angle of attack and moderate cavitation number, the occurrence of cavitation does not always decrease the lift coefficient, because the extension of the cavity, i.e., low pressure region, towards the

downstream direction compensates the decrease of the load near the leading edge. Therefore shorter cavity lengths often lead to smaller lift coefficients.

Figure 14 shows the blade backside pressure coefficient contours at J=0.2 and σ=2.0. It is clearly seen that cavitation is to occur in the tip area. Note that the pressure coefficient in the cavitating area is maintained constant at -σ, as expected from the general cavitation theory. This prediction of cavitation inception can be confirmed by the contours of vapor volume fraction on the backside of the blade, Figure 15, in which the high vapor volume fraction area closely matches the low-pressure area in Figure 14. The computed, iso-surface of vapor volume fraction of 0.1, and observed cavity shapes are compared in Figure 16 at the same condition. Although the tip vortex cavity is missing in the simulation, which is attributed mainly to the mesh resolution in the region, the cavity shape on the blade is in good agreement with each other.

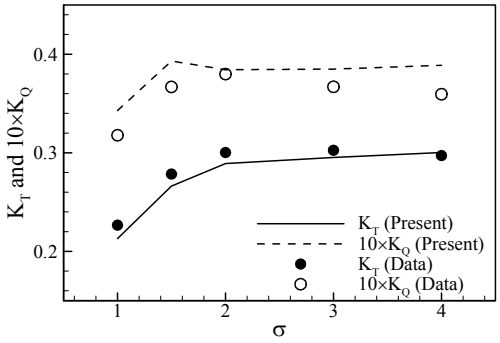

(a) J=0.2

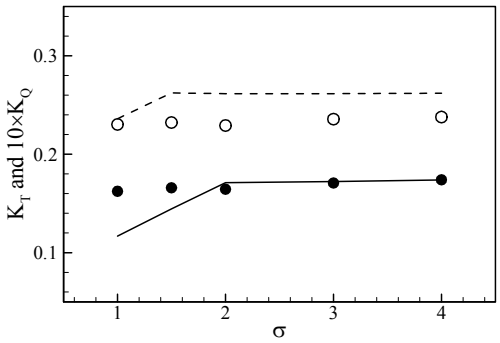

(b) J=0.55

Figure 13 K_T and K_Q vs. σ

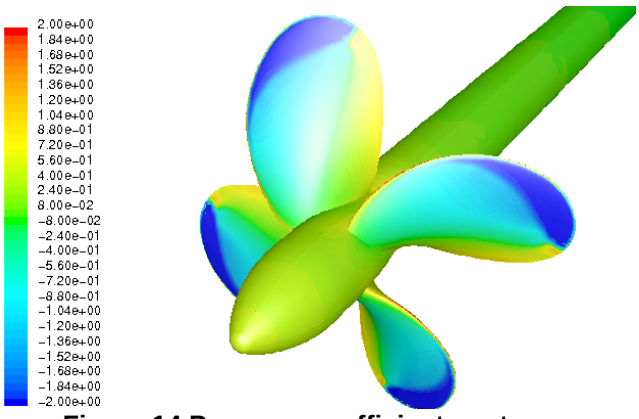

Figure 14 Pressure coefficient contours on back surface at J=0.2 and σ=2.0

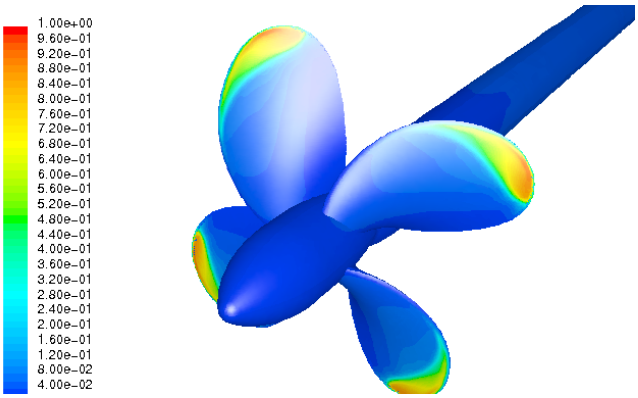

Figure 15. Vapor volume fraction contours on back surface at J=0.2 and σ=2.0

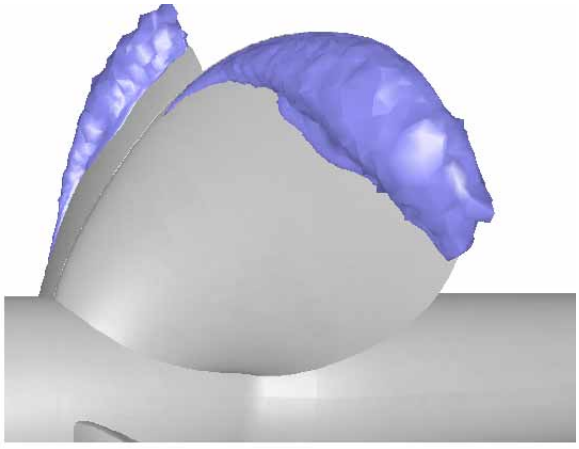

(a) CFD simulation

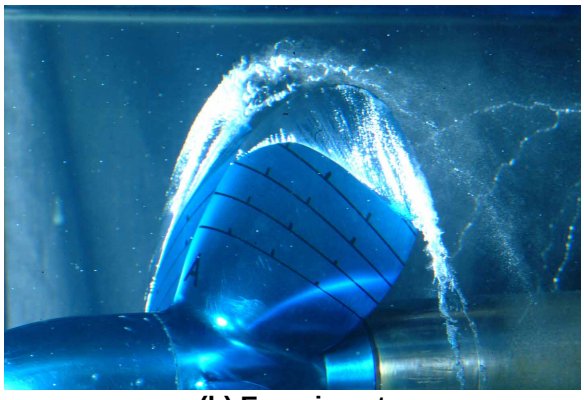

(b) Experiment

Figure 16 Cavity bubble on blades at *J=0.2* and *σ=2.0*

CONCLUSIONS

In this study, we applied RANS approach to steady and unsteady flow around a marine propeller in cavitating and non-cavitating conditions. The unsteady simulation for cavitating condition is being carried out at present, and will be finished by the symposium date.

For steady non-cavitating conditions, the results of the computation were in good agreement with the experimental

data. Although we used a hybrid grid system which mainly consists of tetrahedral cells for easier mesh generation, the accuracy was as good as the computation by Funeno [4] who used a more elaborated block structured grid system. Unsteady flow simulation was also carried out and reasonable agreement was obtained for time-dependent pressure distribution on the blade surface.

Cavitating flow around a propeller was also computed using the cavitation model. Good agreement was obtained in the cavity shape at $J = 0.2$, and variation of K_T and K_Q versus the cavitation number was qualitatively well predicted.

The overall results indicate that RANS approach is applicable to the propeller flow simulation in cavitating and non-cavitating conditions, but further validation and improvement of the models are needed to be used as a reliable tool.

ACKNOWLEDGMENTS

This work was partially financed by the Grant-in-Aid for Scientific Research (No. 14702055) of Ministry of Education, Culture, Sports, Science and Technology. The authors would like to thank Prof. Hajime Yamaguchi for valuable discussions

REFERENCES

[1] Singhal, A.K., Athavale, M.M., Li, H.Y., and Jiang, Y., "Mathematical Basis and Validation of the Full Cavitation Model," *ASME J. Fluids Engineering*, Vol.124, No.3, 2002.

[2] Uto, S. and Kodama, Y., "Application of CFD to the Flow Computation around a Marine Propeller –Grid Generation and Inviscid Flow Computation using Euler Equations- ", J. Kansai Society of Naval Archtects, No. 218, 1992, pp. 171-180.

[3] Funeno, I. and et al., "Analysis of Steady Viscous Flow around a Highly Skewed Propeller (in Japanese)", *J. Kansai Society of Naval Architects*, No. 231, 1999, pp. 1-6.

[4] Funeno, I., "Analysis of Unsteady Viscous Flows around a Highly skewed propeller (in Japanese)", *J. Kansai Society of Naval Architects*, No. 237, 2002, 2002, pp. 39-45.

[5] Funeno, I., "On Inception of Tip Vortex Cavitation of Marine Propellers (in Japanese)", *J, Kansai Society of Naval Architects*, No237, 2002, pp. 47-54.

[6] Funeno, I., "On Viscous Flow around Marine Propellers – HubVortex and Scale Effect-", *Proceedings of New S-Tech 2002 (Third Conference for New Ship and Marine Technology)*, 2002, pp. 17-26.

[7] Kubota, A., Kato, H., and Yamaguchi, H., "A new modeling of cavitating flows: a numerical study of unsteady cavitation on a hydrofoil section," *J. of Fluid Mechanics*, Vol.240, 1992, pp.59-96.

[8] Fluent 6.1 User's Guide, Fluent Inc.

[9] Kim, S.-E., Mathur, S.R., Murthy, J.Y., and Choudhury, D., "A Reynolds-Averaged Navier-Stokes Solver Using Unstructured Mesh-Based Finite-Volume Scheme," AIAA Paper 98-0231, *36th AIAA Aerospace Sciences Meeting and Exhibit*, Reno, NV, 1998.

[10] Kim, S.-E., Rhee, S.H., and Cokljat, D., "Application of Modern Turbulence Models to Vortical Flow Around a 6:1 Prolate Spheroid at Incidence," AIAA Paper 2003-0429, *41st AIAA Aerospace Sciences Meeting and Exhibit*, Reno, NV, 2003.

[11] Wilcox, D.C., *Turbulence Modeling for CFD*, 2nd Ed., DCW Industries, Inc., La Canada, CA, 1998.

[12] Yamaguchi, H., Kato, H., Kamijo, A., and Maeda, M., "Development of marine propellers with better cavitation performance - 2nd report: Effect of design lift coefficient for propellers with flat pressure distribution," *J. of The Society of Naval Architects of Japan*, Vol. 163, 1988.

[13] Ukon, Y., Kurobe, Y. and Kudo, T., "Measurement of Pressure Distribution on a Conventional and a Highly Skewed Propeller Model –Under Non-Cavitating Condition- (in Japanese)", *Journal of the Society of Naval Architects of Japan*, Vol.165, 1989, pp. 83-94.

[14] Heinrich S., "Numerical Prediction of Viscous Propeller Flows", *Schiffstechnik, Ship Technology Research*, Vol. 46, 1999, pp. 35-42.

[15] Koyama, K., "A Numerical Analysis for the Lifting Surface Theory of a Marine Propeller (in Japanese)", *Journal of the Society of Naval Architects of Japan,* Vol. 132, 1972, pp. 91-98.